ANNALS OF GEOPHYSICS, 68, 5, DM556, 2025; doi:10.4401/ag-9329
OPEN ACCESS

Visualizing wavefields with AdriaArray

Johannes Stampa[*,1,2], Felix Eckel[1], Thomas Meier[1]

(1) Kiel University, Institute of Geosciences, Kiel, Germany
(2) University of Cambridge, Department of Earth Sciences, Bullard Laboratories, Cambridge, United Kingdom

Article history: received March 6, 2025; accepted August 14, 2025

Abstract

Large seismic networks like AdriaArray consisting of more than 1000 stations enable new techniques for the visualization and analysis of seismic wave fields. With inter-station distances of less than 40 km, entire wavefields of regional and teleseismic events can be imaged and depicted as animations. In this study we use common data processing techniques applied to data of AdriaArray and neighbouring networks to showcase the propagation of body and surface waves in space and time. A normalization approach based on a low pass filtered envelope assures that both body waves of smaller amplitudes as well as surface waves with large amplitudes are equally distinguishable in the animations. Examples are given for the 7.5 Magnitude 2024 Noto and the 7.8 Magnitude 2023 Turkey earthquakes. Regional effects of wave front deflections, reflections and returning body and surface waves are easily identifiable when comparing with theoretical arrival times. The effect of the station density on the measurement of wavefields is discussed. We show that these animations are well suited to improve the understanding of seismic waves among both seismologists and the general public.

Keywords: Wave fields; Animation; Body Waves; Surface Waves; Adria Array

1. Introduction

During the last two decades, the number of operational seismic stations worldwide has increased dramatically, especially in North America and Europe. Large scale experiments such as the USArray deployment from 2007 to 2018 (Meltzer et al., 1999; IRIS Transportable Array, 2003), the AlpArray temporary network from 2015 to 2022 (Hetényi et al., 2018) and the AdriaArray network from 2022-2025 (Kolínský et al., 2025) are contributing massively to the availability of seismic data in these regions. In this work, we focus on the AdriaArray network which is shown in Fig. 1.

In contrast to the earlier USArray, the stations of AlpArray and AdriaArray are operating concurrently. This results in exceptionally dense station coverage over a large region, i.e. the broad surroundings of the Alpine arc and the Adriatic plate.

The station coverage represents a great opportunity to detect, locate and characterize seismic events and to explore the sub-surface structure of the region from the crust to the core with various methods of seismic tomography, using earthquake data and ambient noise, receiver functions and scattered wave analyses. Additionally, such dense station coverage allows the visualization of the character and spatial-temporal evolution of seismic

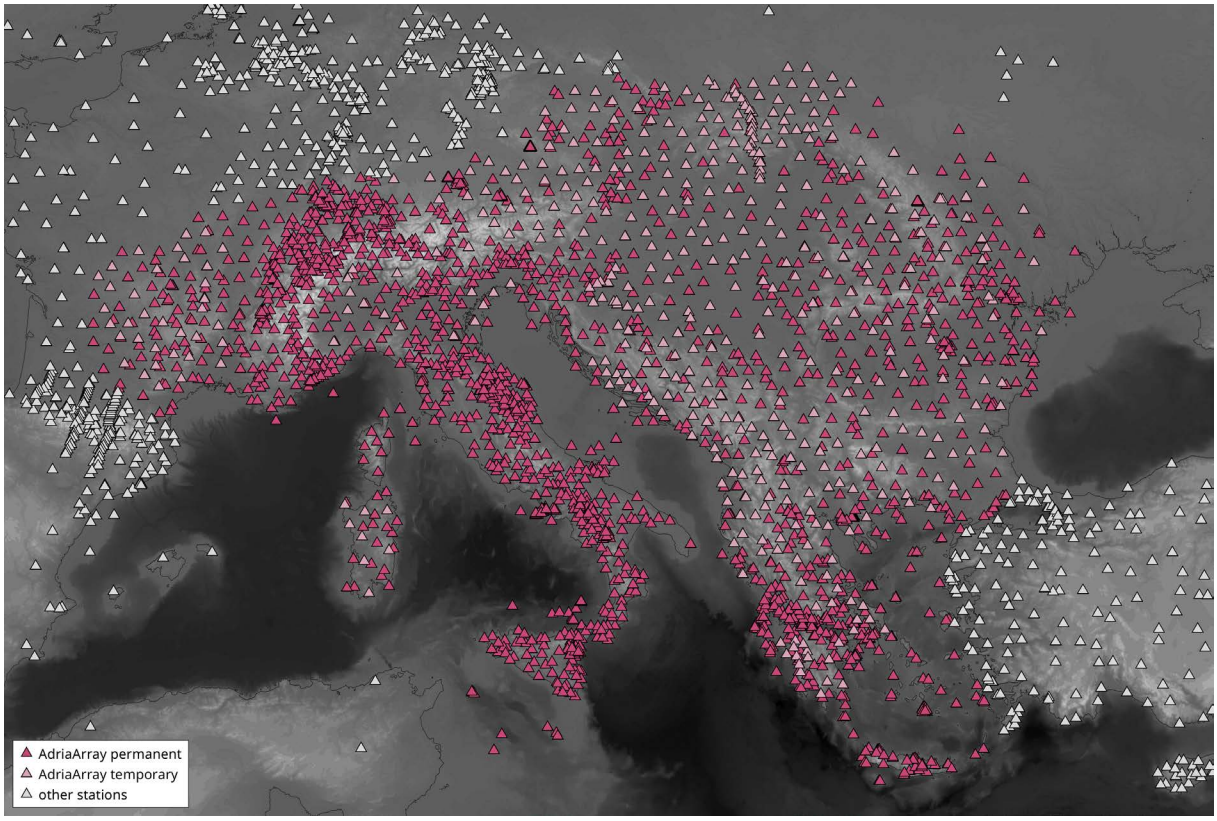

Figure 1. AdriaArray Station Map. The pink stations mark the extend of the virtual AdriaArray network (modified after Kolínský, 2023).

phenomena, for example the propagation and deformation of seismic wave fronts for different body and surface wave phases across the array (e.g. Tesch et al., 2022; Ling et. al. 2021; Trabant et al., 2012).

For this work, the waveform data for two large earthquakes is presented as snapshots of animations depicting the amplitude and particle motion for the location of the stations at each time step. The waveforms are normalized in relation to each other, and also with respect to a low frequency envelope of the individual waveforms, to make faint later phases visible. For each event, a set of two animations is produced, showing the vertical component data as well as the combined horizontal component data, respectively.

In this animated form the data provides an opportunity to gain an intuitive understanding of the propagation of seismic waves, for seismologists as well as the general public. Moreover, these animations can be a valuable tool for science communication efforts, serving as an illustration of the underlying concepts of seismological work. The animations provide a simple way to gain a first impression of the rather complicated topic of seismic wave propagation and could in this way serve as an entry point into seismological topics.

2. Waveform Selection and Acquisition

Two large recent earthquakes were chosen to show the seismic arrivals as recorded by the broad-band seismometers of the AdriaArray. The first is the 2023 Turkey-Syria earthquake that struck central southern Turkey on 6 February at 01:17 UTC with a magnitude of 7.8 Mw (Dal Zilio and Ampuero, 2023). The second is the 2024 Noto earthquake that occurred offshore Japan on 1 January at 07:10 UTC with a magnitude of 7.5 Mw (Yuhi et al., 2024).

The data presented is publicly available in the European Integrated Data Archive (EIDA), operated by Observatories and Research Facilities for European Seismology (ORFEUS) (Strollo et al., 2021), via web services using the Python ObsPy library (Beyreuther et al., May/June 2010). The waveform data is organized in 4-hour segments for each station, starting at the source time of the respective events. In total, 1418 Z-component waveforms and 1449 E- and

N-component waveforms each were downloaded for the 2023 Turkey-Syria earthquake, as well as 1353 Z-component waveforms and 829 E- and N- component waveforms for the 2024 Noto earthquake.

3. Data Processing

The data processing and animation procedure follows the approach presented by Tesch et al. (2022). Additionally, the horizontal components are shown as well.

A Butterworth bandpass-filter with corner periods of 50 s to 200 s is applied to the individual waveforms. The envelope of this filtered waveform y^* is then calculated as the absolute values of the analytic signal with an imaginary part representing the Hilbert transform of the real part (Červený and Zahradník, 1975):

$$E(t) = \left| y(t) - iH\left(y^*(t)\right) \right| \tag{1}$$

A lowpass Butterworth filter with corner frequency 1/100 s is applied to this envelope. The filtered waveform is then normalized at each sample with the corresponding value of this filtered envelope E^*:

$$y(t) = \frac{y^*(t)}{E^*(t)} \tag{2}$$

This makes later phases visible, by continuously adjusting the dynamic range over the whole length of the recording to ensure maximum contrast without requiring clipping of the signal. However, during periods where no signal is present, the amplitude of the noise will be increased as well, and the amplitudes of phases at different times can no longer be compared to each other.

The individual waveforms are then aligned to each other. Since only one frame for each second is drawn, the waveforms are decimated to the chosen time steps.

4. Wavefield animations

The processed waveforms are drawn on a background map showing the topography according to the ETOPO1 global relief model (Amante and Eakins, 2009). For each time step, the waveform at the corresponding sample is drawn as a circle at the corresponding station location. The scaled amplitude is represented as the size and color saturation of the circular station marker, and the polarity of the amplitude is encoded as the color of the marker. For vertical waveform animations, red represents positive amplitudes and blue represents negative amplitudes. For the horizontal waveform animations, the horizontal polarity direction is encoded in a continuous color wheel, with white and black representing motion with radial polarity along or opposite to the propagation direction, and blue and red standing for transverse polarity, to the left and to the right of the direction of wave propagation, respectively. This color wheel is shown in the top right corner, with an alignment representative for the location of a reference station. Because horizontal motions are indicated by color instead of shifting the station symbol, also snapshots of animations are informative.

The reference station near the center of the map is indicated by a triangle. The original vertical component or horizontal waveforms recorded at the reference station are drawn in white, at the bottom of the map. The time progress is marked by this waveform being colored orange, and the timestamp for the recording is given in the bottom left. Small circles are drawn centered on the event epicenter, with an even spacing of 4°, to facilitate identifying deflections and deformation of the wave fronts passing the array.

Additionally, the theoretical wave fronts for arriving body wave phases are calculated with TauPy (Crotwell et al., 1999). They are added to the animations to enable identifying the arriving seismic phases. The wave fronts for Love and Rayleigh surface waves are also estimated using representative group velocities for which 50 to 80 s. They are likewise shown in the animations.

4.1 2024 Noto earthquake

In this section, snapshots of the animations of the waveform recordings during the arrival of various teleseismic phases originating from the 2024 Noto earthquake are shown. The vertical and horizontal components are given alongside each other.

Figure 2 shows the first arriving P- and the PcP-phase, about 12 minutes after the main shock of the earthquake. The array is almost at the distance where the two phases merge, and transition then into the Pdiff-phase. The initial onset has already passed over the array, and the first zero crossing of the arriving waveform is just moving over the reference station. The wavefront appears very coherent for the vertical component. For the horizontal components, the image is a bit less coherent, but there is still a clear wavefront in particular for the first phase visible in red in the vertical component. This wavefront shows up as a white and black contrast, which signifies amplitudes of the radial horizontal component of the recording, i.e. radial polarization of the wavefield. The P-waves show up in the horizontal components due to the fact that the wave incidence is not perfectly vertical, so that a part of the radial component of the body wave is picked up by the horizontal components.

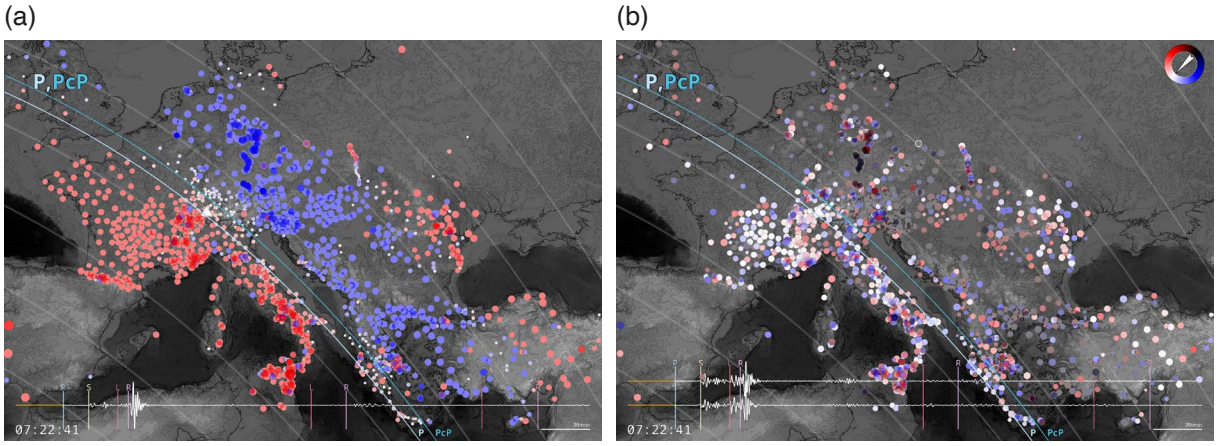

Figure 2. Snapshots of the animations for the vertical (a) and horizontal (b) component waveform data of the 2024 Noto earthquake, showing the arrival of the P- and PcP-phases.

The arrival of the S-, ScS-, SKS-, PS- and PPS-phases is shown in Fig. 3. This is about 21 minutes after the mainshock. Both the vertical and the horizontal components show clear wavefronts. Remarkably, the apparent horizontal wavelength of the wavefield at the surface seems to differ, with the vertical components showing

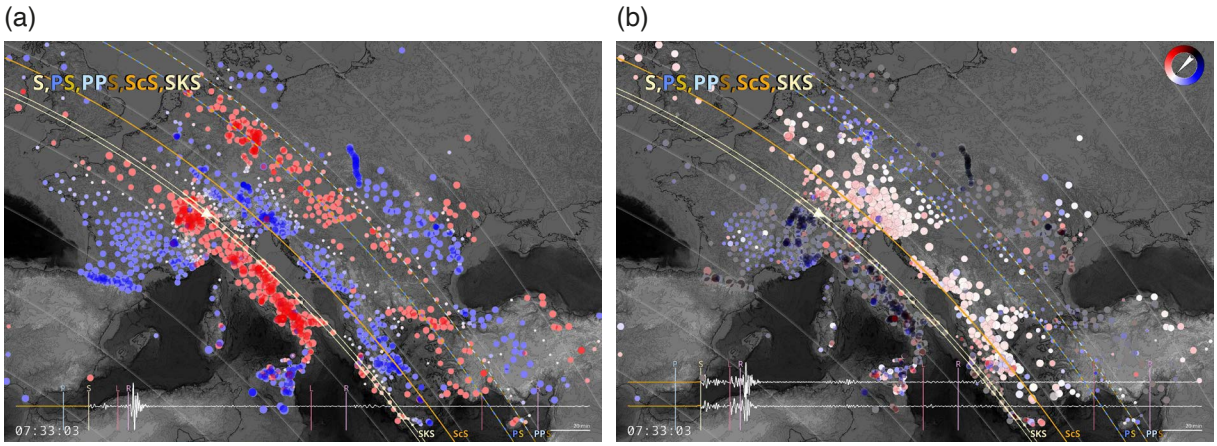

Figure 3. Snapshots of the animations for the vertical (a) and horizontal (b) component waveform data of the 2024 Noto earthquake, showing the arrival of the S-, ScS-, SKS-, PS- and PPS-phases.

a shorter apparent horizontal wavelength compared to the horizontal components indicating that for this example the horizontal particle motion is less variable than the vertical one. The S- and SKS-phase appear directly on top of each other, with the ScS-phase close behind, followed by the PS- and PPS-phases. The polarization direction of the main S-phase wavefront is predominantly radial, which is indicated by the amplitudes being shaded in white and black, with only a small transversal part, which is showing up as slight red and blue hues.

In Fig. 4, the arrival of the Love wave is shown, appearing as coherent bands of red and blue in the horizontal components. This is due to the transverse polarization of the Love waves. The vertical component appears less coherent, but the wavefronts are still clearly visible. Love waves in isotropic laterally homogeneous media are confined to the horizontal components and zero on the vertical component. There are however observations of so-called quasi-Love waves with significant coherent vertical components in the Love wave time window that may be caused by anisotropy or scattering due to lateral variations in the isotropic or anisotropic structure (e.g. Park et al., 1992; Meier et al., 1997; Levin et al., 2007; Eakin, 2021). Waves visible in the snapshot of the vertical component may alternatively be associated with higher multiples of P and S-phases. In this case the wavefield on the vertical component should however be less coherent with the horizontal components.

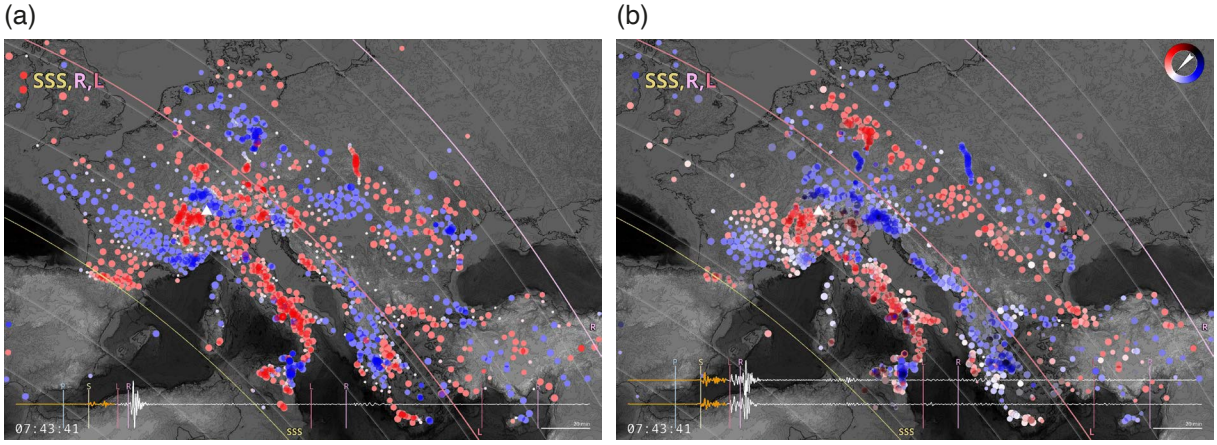

Figure 4. Snapshots of the animations for the vertical (a) and horizontal (b) component waveform data of the 2024 Noto earthquake, showing the arrival of the Love wave.

The arrival of the Rayleigh wave in Fig. 5 marks another change in the polarization direction on the horizontal components. As expected for Rayleigh waves, they are radially polarized, showing up as white and black stripes (Fig. 5b). They consequently show up clearly in both the horizontal and vertical components, with a horizontal wavelength that is about half of that of the Love waves.

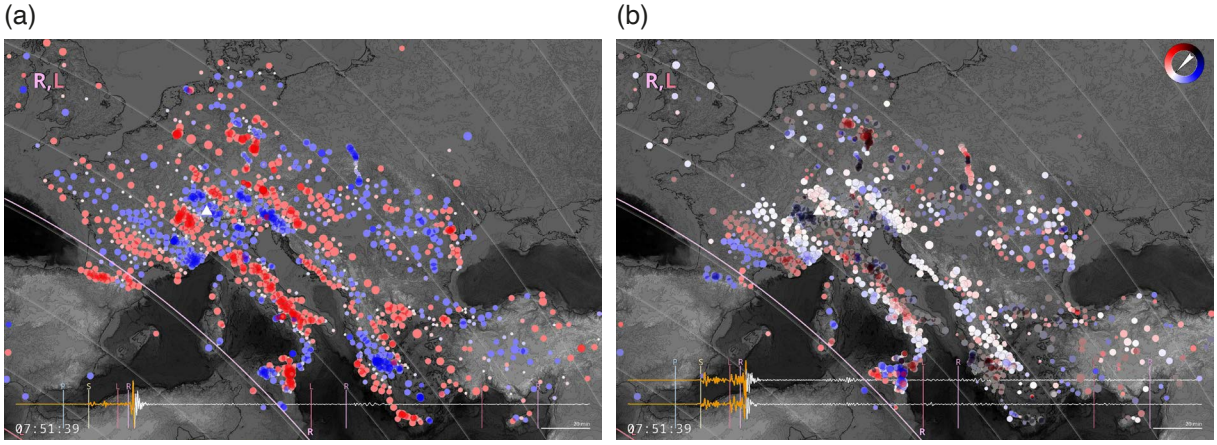

Figure 5. Snapshots of the animations for the vertical (a) and horizontal (b) component waveform data of the 2024 Noto earthquake, showing the arrival of the Rayleigh wave.

4.2 2023 Turkey-Syria earthquake

In this section, snapshots of the animations of the waveform recordings during the initial phase of the 2023 Turkey-Syria earthquake, and the subsequent return of the teleseismic phases that have completed a full lap around the Earth are shown. The vertical and horizontal components are shown alongside each other.

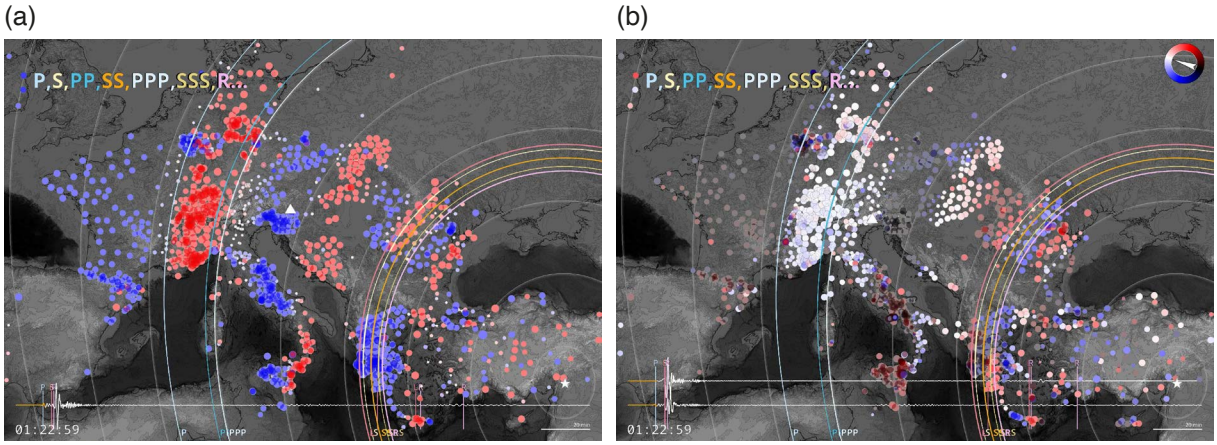

Figure 6. Snapshots of the animations for the vertical (a) and horizontal (b) component waveform data of the 2023 Turkey-Syria earthquake, showing the initial wavefield propagation across the array.

Figure 6 shows the wave field over the array about 5 minutes after the main shock of the earthquake. The wave front of the P-phase can be identified going from north to south through the eastern part of France. It appears as the boundary between blue and red colours in the vertical and as the boundary between dark and light colours in the horizontal components. At this distance from the epicenter, it is so closely followed by its surface reflected multiples that these phases cannot be distinguished. In the horizontal components, it shows strong polarization in radial direction as expected (black and white colors). The wave front of the S-phase, indicated by the beige small circle, is buried in the Love wave, indicated by the pink small circle, which barely precedes it at this distance. For this reason, the horizontal components show a clear band of transversal polarization here (red and blue).

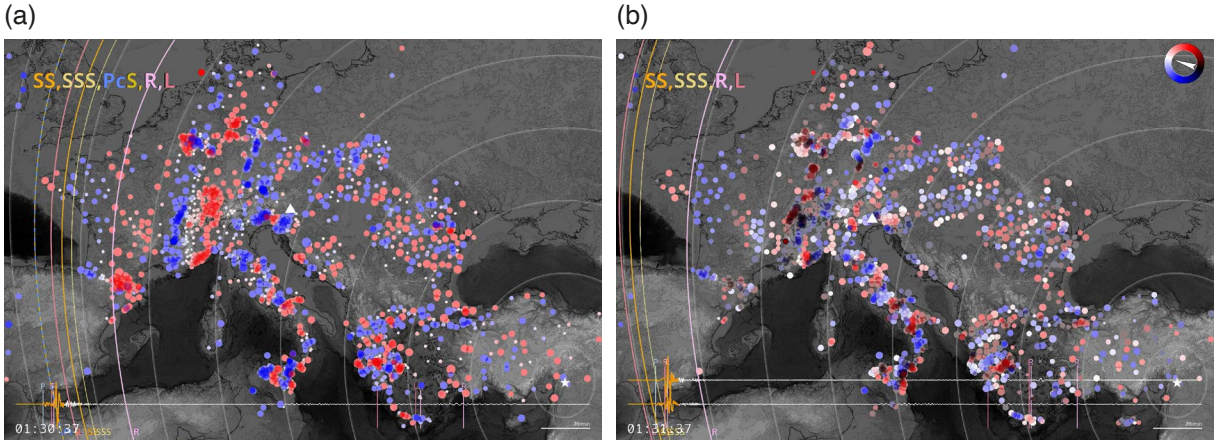

Figure 7. Snapshots of the animations for the vertical (a) and horizontal (b) component waveform data of the 2023 Turkey-Syria earthquake, showing the coda of the Rayleigh wave.

In Fig. 7, the coda of the Rayleigh wave is shown. The horizontal wavelength of the wavefield varies across the array, with wavelengths appearing shorter closer to the epicenter in this snapshot. This is due to the Rayleigh wave

exhibiting dispersion, i.e. frequency dependence in the propagation velocity of the seismic wave. In the region close to the epicenter, in Turkey, Greece, North Macedonia, Bulgaria and Romania, wavelengths are shorter and seem to be clockwise inclined with respect to the small circles around the epicenter. Aliasing effects due to the small wavelength may, however, contribute to this visual impression.

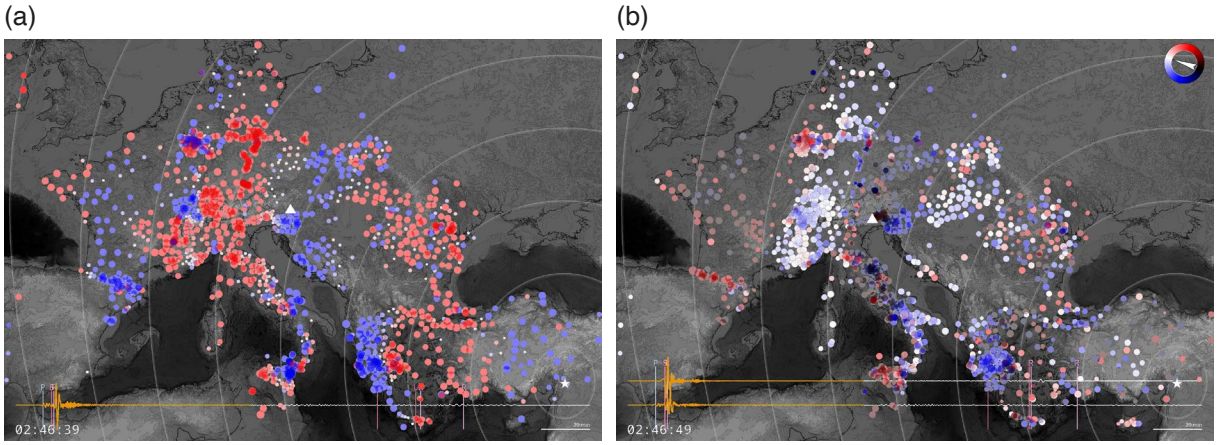

Figure 8. Snapshots of the animations for the vertical (a) and horizontal (b) component waveform data of the 2023 Turkey-Syria earthquake, showing returning body waves.

Figure 8 shows a snapshot from the animation about 90 minutes after the main shock. Wavefronts arriving from the opposite direction of the initial wave field are appearing in both the vertical and horizontal components. These are returning body wave phases that have completed a full lap of the Earth's circumference. Judging from the radial polarization apparent from the horizontal components, these are most likely surface reflected multiples of the P-wave.

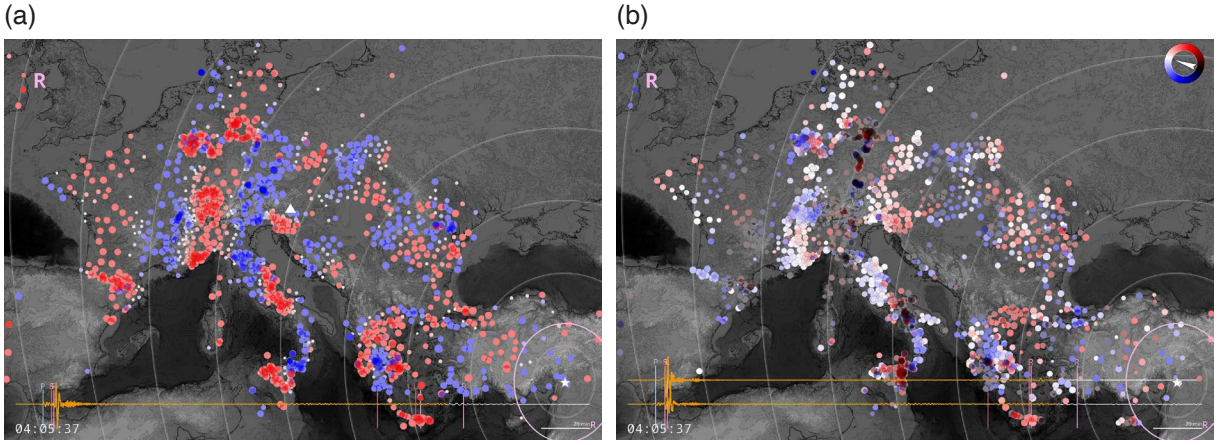

Figure 9. Snapshots of the animations for the vertical (a) and horizontal (b) component waveform data of the 2023 Turkey-Syria earthquake, showing returning Rayleigh surface wave.

Finally, Fig. 9 shows the returning Rayleigh wave a bit less than 3 hours after the main shock. The wave field appears remarkably coherent. The incidence of the wave fronts is reversed, similar to the case for the returning body waves, since the surface waves imaged in this screen shot have completed the full lap around the Earth. The apparent period of the Rayleigh wave is longer; the higher frequencies having been attenuated along the way.

5. Conclusions

The snapshots presented in this work provide an intuitive insight in the propagation of seismic waves. Time dependent amplitude scaling is necessary to visualize also small amplitude phases. Wave fields appear coherent, even after a full lap around the Earth. With the color wheel encoding for the horizontal components, it is even possible to distinguish differences in polarization between different parts of the wave field, seen most vividly in the difference between Love and Rayleigh waves. This holds also for snapshots because the color is varied and not the position of the symbol. The theoretical phase wave fronts provide a guide to identify the most important seismic phases. The reference waveform at the bottom provides information on the amplitudes of the wavefield.

The animations also serve to demonstrate the capabilities of the AdriaArray, showcasing the station density and data quality achieved by the cooperation of the participating institutions. Concerning data quality assurance, these animations are useful for providing a comprehensive first look at the data. This could in turn enable researchers to identify problematic stations in the data set, e.g. timing or instrument polarity issues. The procedures we developed for creating these animations could be adapted to specific requirements for quality testing, for example implementing a different normalization scheme.

Data availability statement. The permanent and temporary stations are contributed via the following networks codes: 1J (Moretti et al., 2021), 1N (Malet et al., 2015), 1Y (Friederich et al., 2022), 2Y (Pesaresi and Rossi, 2022), 3D (Alparone et al., 2021), 4P, 6E (Dahm et al., 2023), 7C (Constanzo et al., 2022), 8C (Helmstetter et al., 2020), 8D (SED, 2005), 9H, AC (IGEO, 2002), BQ (Bensberg Observatory, 2016), BS (BAS, 1980), BW (LMU, 2001), C4 (CERN, 2016), CA (ICGC, 1984), CH (SED, 1983), CL (CRLAB and RESIF, 2013), CQ (GSD, 2013), CR (UNIZG, 2001), CZ (Czech, 1973), DK (GEUS, 1976), EI (DIAS, 1993), ES (IGN, 1999), FO (Epos, 2020), FR (Epos, 1962), G (IPGP and EOST, 1982), GB (BGS, 1970), GE (GEOFON, 1993), GQ, GR (BGR, 1976), GU (UNIGE, 1967), GX, HA (UOA, 2008), HC (HMU, 2006), HL (NOA, 1975), HP (UPATRAS, 2000), HS (HLNUG, 2012), HT (AUTH, 1981), HU (MTA CSFK GGI KRSZO, 1992), IV (INGV, 2005), IX, IY (UNICAL, 1981), KO (KOERI, 1971), KQ (CAU, 2017), MD (IGS ASM, 2007), ME (HMZCG, 1982), ML (UM 2014), MN (Mednet, 1990), MT (OMIV and RESIF, 2006), NI (OGS and UNITS, 2002), NL (KNMI, 1993), OE (ZAMG, 1987), OT (UNIBA, 2013), OX (OGS, 2016), PL (PAN, 1990), PM (IPMA, 2006), RD (RESIF, 2018), RF (UNITS, 1993), RO (NIEP, 1994), SI, K (ESI SAS, 2004), SL (ARSO, 1990), ST (TRENTO, 1981), SX (UNILE, 2001), TH (IGW, 2009), TU (AFAD, 1990), TV, UD (GCSK, 2010), VM (INGV, 2023), WM (ROA et al., 2996), XE (Chiarabba et al., 2022), XP (Paul et al., 2023), Y5 (Obermann et al., 2022), Y8 (Neagoe, 2022), Z6 (Schlömer et al., 2022). The seismic data used in this study can be downloaded from EIDA. Some data from the AdriaArray initiative becomes publicly available two years after acquisition. The animations can be downloaded at: https://cloud.rz.uni-kiel.de/index.php/s/bApBnArMGmmwnxa.

Acknowledgements. We acknowledge the personnel responsible for recording, storing and distributing the data at EIDA, ORFEUS, the data centers and the network operators. Parts of this work has been funded by ORFEUS and DFG (ME 1320/9-1) grants.

References

Alparone, S., O. M. G. Cocina, D. Contrafatto, G. Larocca et al. (2021). Seismic Data acquired by the INGV temporary network for seismic monitoring of the island of Vulcano to increase volcanic activity (Sicily, Italy) – 2021 (Data set), Istituto Nazionale di Geofisica e Vulcanologia (INGV), doi:10.13127/sd/cfz7ftsw-y.

Amante, C. and B. W. Eakins (2009). Etopo1 arc-minute global relief model: procedures, data sources and analysis, doi:10.7289/V5C8276M.

Aristotle University of Thessaloniki, AUTH (1981). Aristotle University of Thessaloniki Seismological Network (Data set), International Federation of Digital Seismograph Networks, doi:10.7914/SN/HT.

Beyreuther, M., R. Barsch, L. Krischer, T. Megies et al. (2010). Obspy: A Python toolbox for seismology, Seismol. Res. Lett., 81, 3, 530-533, doi:10.1785/gssrl.81.3.530.

British Geological Survey, BGS (1970). Great Britain Seismograph Network (Data set), International Federation of Digital Seismograph Networks, doi:10.7914/av8j-nc83.

CERN (2016). CERN Seismic Network, ETH Zurich, doi:10.12686/sed/networks/c4.

Červený, V. and J. Zahradník (1975). Hilbert transform and its geophysical applications, Acta Univ. Carolin. Math. Phys., 16, 1, 67-81.

Charles University in Prague (Czech), Institute of Geonics, Institute of Geophysics, Academy of Sciences of the Czech Republic et al. (1973). Czech Regional Seismic Network (Data set), International Federation of Digital Seismograph Networks, doi:10.7914/SN/CZ.

Chiarabba, C., A. Costanzo, P. De Gori, P. Del Gaudio et al. (2022). Pollino Broad-Band Near Fault Observatory (2022-2033), Southern Italy (Data set), Istituto Nazionale di Geofisica e Vulcanologia, INGV, doi:10.13127/sd/ns6hb3q8ve.

Christian Albrechts – Universitat zu Kiel, CAU (2017). Kiel University Earthquake Monitoring (Data set), International Federation of Digital Seismograph Networks, doi:10.7914/SN/KQ.

Corinth Rift Laboratory Team CRLAB and RESIF Datacenter (2013). CL – Corinth Rift Laboratory Seismological Network, CRLNET (Data set), RESIF – Réseau Sismologique et Géodésique Français, doi:10.15778/RESIF.CL.

Costanzo, A., S. Falcone, C. La Piana, A. Caserta et al. (2022). Urban Seismic Network (RUSN-CAL-INGV) – Real time Urban Seismic Network managed by CALabrian headquarters of INGV for monitoring urban areas, critical infrastructures and cultural heritage sites (Data set), Istituto Nazionale di Geofisica e Vulcanologia, INGV, doi:10.13127/sd/o5nrhmp9n7.

Crotwell, H. P., T. J. Owens and J. Ritsema (1999). The TauP Toolkit: Flexible Seismic Travel-time and Ray-path Utilities, Seismol. Res. Lett., 70, 2, 154-160, doi:10.1785/gssrl.70.2.154.

Dahm, T., M. P. Isken, C. Milkereit, S. Mikulla et al. (2023). Eifel Large-N Seismic Network, ELSN (Data set), GFZ Data Services, doi:10.14470/1R080930.

Dal Zilio, L. and J. P. Ampuero (2023). Earthquake doublet in turkey and syria, Commun. Earth Environ., 4, 1, 71, doi:10.1038/s43247-023-00747-z.

Department of Earth and Environmental Sciences, Geophysical Observatory, University of Munchen, LMU (2001). BayernNetz (Data set), International Federation of Digital Seismograph Networks, doi:10.7914/SN/BW.

Department of Geosciences, Bensberg Observatory, University of Cologne (2016). Bensberg Earthquake Network (Data set), International Federation of Digital Seismograph Networks, doi:10.7914/SN/BQ.

Disaster and Emergency Management Authority, AFAD (1990). Turkish National Seismic Network (Data set), Department of Earthquake, Disaster and Emergency Management Authority, doi:10.7914/SN/TU.

Dublin Institute for Advanced Studies, DIAS (1993). Irish National Seismic Network (Data set), International Federation of Digital Seismograph Networks, doi:10.7914/SN/EI.

Eakin (2021). Quasi-Love wave scattering reveals tectonic history of Australia and its margins reflected by mantle anisotropy, Commun. Earth Environ., 2, 210, doi:10.1038/s43247-021-00276-7.

Epos-France (1962). Epos-France Broad-band network, RLBP (Data set), Epos-France Seismological Data Centre, doi:10.15778/RESIF.FR.

Epos-France Seismology (2020). French Associated Seismological Network (Data set), Epos-France Seismological Data Centre, doi:10.15778/resif.fo.

ESI SAS, Former GPI SAS, Geophysical Institute Of The Slovak Academy Of Sciences (2004). National Network of Seismic Stations of Slovakia (Data set), GFZ Data Services, doi:10.14470/FX099882.

Federal Institute for Geosciences and Natural Resources, BGR (1976). German Regional Seismic Network, GRSN, Bundesanstalt für Geowissenschaften und Rohstoffe, doi:10.25928/mbx6-hr74.

French Landslide Observatory – Seismological Datacenter OMIV / RESIF (2006). Observatoire Multi-disciplinaire des Instabilités de Versants (Data set), RESIF – Réseau Sismologique et Géodésique Français, doi:10.15778/RESIF.MT.

Friederich, W., C. Evangelidis, C. Papazachos, E. Sokos et al. (2022). AdriaArray Temporary Network: Greece, North Macedonia (Data set), International Federation of Digital Seismograph Networks, doi:10.7914/y0t2-3b67.

GEOFON Data Centre (1993). GEOFON Seismic Network (Data set), GFZ Data Services, doi:10.14470/TR560404.

Geological and Seismological Institute of Moldova, IGS ASM (2007). Moldova Digital Seismic Network (Data set), International Federation of Digital Seismograph Networks, doi:10.7914/SN/MD.

Geological Survey Department Cyprus, GSD (2013). Cyprus Broadband Seismological Network (Data set), International Federation of Digital Seismograph Networks, doi:10.7914/SN/CQ.

Geological Survey-Provincia Autonoma di Trento, TRENTO (1981). Trentino Seismic Network (Data set), International Federation of Digital Seismograph Networks, doi:10.7914/SN/ST.

GEUS Geological Survey of Denmark and Greenland (1976). Danish Seismological Network (Data set), International Federation of Digital Seismograph Networks, doi:10.7914/nw3x-df02.

Helmstetter, A., P. Guéguen and RESIF (2020). Seismic network 8C: monitoring swarms in the Mont-Blanc and Vallorcine area, RESIF – SISMOB (Data set), RESIF – Réseau Sismologique et Géodésique Français, doi:10.15778/RESIF.8C2019.

Hetényi, G., I. Molinari, J. Clinton, G. Bokelmann et al. (2018). The AlpArray seismic network: a large-scale European experiment to image the Alpine orogen, Surv. Geophys., 39, 1009-1033, doi:10.1007/s10712-018-9472-4.

Hessian Agency for Nature Conservation, Environment and Geology, HLNUG (2012). Hessischer Erdbebendienst (Data set), International Federation of Digital Seismograph Networks, doi:10.7914/SN/HS.

Institut Cartogràfic i Geològic de Catalunya, ICGC (1984). Catalan Seismic Network (Data set), International Federation of Digital Seismograph Networks, doi:10.7914/SN/CA.

Institut de physique du globe de Paris – IPGP and École et Observatoire des Sciences de la Terre de Strasbourg – EOST (1982). GEOSCOPE, French Global Network of broad band seismic stations, Institut de physique du globe de Paris (IPGP), Université de Paris, doi:10.18715/GEOSCOPE.G.

Institut fuer Geowissenschaften-IGW, Friedrich-Schiller-Universitaet Jena. (2009). Thüringer Seismologisches Netz (Data set), International Federation of Digital Seismograph Networks, doi:10.7914/SN/TH.

Institute of Geophysics, Polish Academy of Sciences, PAN (1990). Polish Seismological Network (Data set), International Federation of Digital Seismograph Networks, doi:10.7914/90rh-0q80.

Institute of GeoSciences-IGEO, Polytechnic University of Tirana (2002). Albanian Seismological Network (Data set), International Federation of Digital Seismograph Networks, doi:10.7914/SN/AC.

Instituto Geografico Nacional-IGN (1999). Spanish Digital Seismic Network (Data set), International Federation of Digital Seismograph Networks, Spain, doi:10.7914/SN/ES.

Instituto Português do Mar e da Atmosfera-IPMA (2006). Portuguese National Seismic Network (Data set), International Federation of Digital Seismograph Networks, doi:10.7914/SN/PM.

Istituto Nazionale di Geofisica e Vulcanologia, INGV (2005). Rete Sismica Nazionale-RSN (Data set), Istituto Nazionale di Geofisica e Vulcanologia, doi:10.13127/sd/x0fxnh7qfy.

Istituto Nazionale di Geofisica e Vulcanologia, INGV (2023). Seismic Data acquired by Marche Seismic Network-MSN (Data set). Istituto Nazionale di Geofisica e Vulcanologia, doi:10.13127/sd/z7hoi9u3ix.

Istituto Nazionale di Oceanografia e di Geofisica Sperimentale – OGS (2016). North-East Italy Seismic Network (Data set), FDSN, doi:10.7914/SN/OX.

Istituto Nazionale di Oceanografia e di Geofisica Sperimentale – OGS and University of Trieste – UNITS (2002). North-East Italy Broadband Network (Data set), International Federation of Digital Seismograph Networks, doi:10.7914/SN/NI.

IRIS Transportable Array (2003). USArray transportable array, doi:10.7914/SN/TA.

Kandilli Observatory And Earthquake Research Institute-KOERI, Boğaziçi University (1971). Kandilli Observatory and Earthquake Research Institute (Data set), International Federation of Digital Seismograph Networks, doi:10.7914/SN/KO.

KNMI (1993). Netherlands Seismic and Acoustic Network, Royal Netherlands Meteorological Institute – KNMI, doi:10.21944/e970fd34-23b9-3411-b366-e4f72877d2c5.

Kolínský, P., T. Meier, M. Agius, A. Bijedić et al. (2025a). AdriaArray – a Passive Seismic Experiment to Study Structure, Geodynamics and Geohazards of the Adriatic Plate, Ann. Geophys., 68, this Issue.

Kolínský, P., J. Stampa, L. Vecsey, F. Eckel et al. (2025b). Methods for data and metadata quality tests of large dense seismic networks – focus on AdriaArray, Ann. Geophys., 68, this Issue.

Kövesligethy Radó Seismological Observatory, Geodetic and Geophysical Institute, Research Centre For Astronomy and Earth Sciences, Hungarian Academy Of Sciences – MTA CSFK GGI KRSZO (1992). Hungarian National Seismological Network (Data set), GFZ Data Services, doi:10.14470/UH028726.

Levin, V., J. Park, F. P. Lucente, L. Margheriti et al. (2007). End of subduction in northern Apennines confirmed by observations of quasi-Love waves from the great 2004 Sumatra-Andaman earthquake, Geophys. Res. Lett., 34, 4, doi:10.1029/2006GL028860.

Main Center of Special Monitoring, GCSK (2010). Seismic Network Main Center of Special Monitoring (Data set), International Federation of Digital Seismograph Networks, doi:10.7914/SN/UD.

Malet, J. P., C. Hibert, M. Radiguet, S. Gautier et al. (2015). French Landslide Observatory – OMIV, Temporary data, MT-campagne, RESIF – SISMOB (Data set), RESIF – Réseau Sismologique et Géodésique Français, doi:10.15778/RESIF.1N2015.

MedNet Project Partner Institutions (1990). Mediterranean Very Broadband Seismographic Network, MedNet (Data set), Istituto Nazionale di Geofisica e Vulcanologia, INGV, doi:10.13127/sd/fbbbtdtd6q.

Meier, T., S. Lebedev, G. Nolet and F. A. Dahlen (1997). Diffraction tomography using multimode surface waves, J. Geophys. Res., 102, B4, 8255-8267, doi:10.1029/96JB03227.

Meltzer, A., R. Rudnick, P. Zeitler, A. Levander et al. (1999). Usarray initiative, GSA TODAY, 9.

Moretti, M., L. Margheriti, S. Alparone, A. Costanzo et al. (2021). Seismic Data acquired by FocusX temporary land-network – FXland, Southern Italy (Data set), Istituto Nazionale di Geofisica e Vulcanologia, INGV, doi:10.13127/sd/o5qwm6wjcd.

National Institute for Earth Physics, NIEP Romania (1994). Romanian Seismic Network (Data set), International Federation of Digital Seismograph Networks, doi:10.7914/SN/RO.

National Institute of Geophysics, Geodesy and Geography, BAS (1980). National Seismic Network of Bulgaria (Data set), International Federation of Digital Seismograph Networks, doi:10.7914/SN/BS.

National Observatory of Athens – NOA (1975). National Observatory of Athens Seismic Network (Data set), International Federation of Digital Seismograph Networks, Institute of Geodynamics, Athens, doi:10.7914/SN/HL.

Cristian Neagoe (2022). AdriaArray Temporary Network: Bulgaria, Moldova, Poland, Romania, Ukraine (Data set), International Federation of Digital Seismograph Networks, doi:10.7914/b1sc-0n71.

Obermann, A., D. Jozinović, S. Cvijic, A. Krehić et al. (2022). Swiss Contribution to AdriaArray Temporary Network, ETH Zurich, doi:10.12686/SED/NETWORKS/Y5.

Park, J., and Y. Yu (1992). Anisotropy and coupled free oscillations: simplified models and surface wave observations, J. Geophys. Res., 110, 3, 401-420, doi:10.1111/j.1365-246X.1992.tb02082.x.

Paul, A., A. Mordret, C. Aubert, S. Chevrot et al. (2023). MACIV-BB (backbone) temporary broadband experiment in the French Massif Central, France, RESIF-SISMOB (Data set), RESIF – Réseau Sismologique et Géodésique Français, doi:10.15778/RESIF.XP2023.

Pesaresi, D. and G. Rossi (2022). AdriaArray Temporary Network: Italy – northeast (Data set), International Federation of Digital Seismograph Networks, doi:10.7914/1p36-6t87.

RESIF (2018). CEA/DASE broad-band permanent network in metropolitan France (Data set), RESIF – Réseau Sismologique et Géodésique Français, doi:10.15778/RESIF.RD.

San Fernando Royal Naval Observatory-ROA, Universidad Complutense De Madrid-UCM, Helmholtz-Zentrum Potsdam Deutsches GeoForschungsZentrum-GFZ et al. (1996). The Western Mediterranean BB seismic Network (Data set), GFZ Data Services, doi:10.14470/JZ581150.

Schlömer, A., J. Wassermann, J. Plomerová, L. Vecsey et al. (2022). AdriaArray Temporary Network: Albania, Austria, Czech Rep., Germany, Hungary, Kosovo, Montenegro, Slovakia (Data set), International Federation of Digital Seismograph Networks, doi:10.7914/2cat-tq59.

Sector for Seismology, Institute of Hydrometeorology and Seismology of Montenegro, HMZCG (1982). Montenegrin Seismic Network (Data set), International Federation of Digital Seismograph Networks, doi:10.7914/SN/ME.

Slovenian Environment Agency, ARSO (1990). Seismic Network of the Republic of Slovenia (Data set), International Federation of Digital Seismograph Networks, doi:10.7914/SN/SL.

Strollo, A., D. Cambaz, J. Clinton, P. Danecek et al. (2021). EIDA: The European Integrated Data Archive and Service Infrastructure within ORFEUS, Seismol. Res. Lett., 92, 3, 1788-1795, doi:10.1785/0220200413.

Swiss Seismological Service, SED (1983). National Seismic Networks of Switzerland, ETH Zürich, doi:10.12686/sed/networks/ch.

Swiss Seismological Service, SED (2005). Temporary deployments in Switzerland associated with aftershocks and other seismic sequences, ETH Zurich, doi:10.12686/sed/networks/8d.

Technological Educational Institute of Crete, HMU (2006). Seismological Network of Crete (Data set), International Federation of Digital Seismograph Networks, doi:10.7914/SN/HC.

Tesch, M., J. Stampa, T. Meier, E. Kissling et al. (2022). Imaging seismic wave-fields with alparray and neighboring european networks, Int. J. Earth Sci., 1-14, doi:10.1007/s00531-021-02116-7.

Trabant, C., A. R. Hutko, M. Bahavar, R. Karstens et al. (2012). Data Products at the IRIS DMC: Stepping Stones for Research and Other Applications, Seismol. Res. Lett., 83, 5, 846-854, doi:10.1785/0220120032.

Università Della Calabria, UNICAL (1981). Rete Sismica Unical (Data set), International Federation of Digital Seismograph Networks, doi:10.7914/SN/IY.

University of Athens, UOA (2008). Hellenic Seismological Network, University of Athens, Seismological Laboratory (Data set), International Federation of Digital Seismograph Networks, doi:10.7914/SN/HA.

University of Bari Aldo Moro, UNIBA (2013). OTRIONS (Data set), International Federation of Digital Seismograph Networks, doi:10.7914/SN/OT.

University of Genoa, UNIGE (1967). Regional Seismic Network of North Western Italy (Data set), International Federation of Digital Seismograph Networks, doi:10.7914/SN/GU.

University of Leipzig, UNILE (2001). SXNET Saxon Seismic Network (Data set), International Federation of Digital Seismograph Networks, doi:10.7914/SN/SX.

University of Malta, UM (2014). Malta Seismic Network (Data set), International Federation of Digital Seismograph Networks, doi:10.7914/SN/ML.

University of Patras, UPATRAS (2000). University of Patras, Seismological Laboratory (Data set), International Federation of Digital Seismograph Networks, doi:10.7914/SN/HP.

University of Trieste, UNITS (1993). Friuli Venezia Giulia Accelerometric Network (Data set), International Federation of Digital Seismograph Networks, doi:10.7914/SN/RF.

University of Zagreb, UNIZG (2001). Croatian Seismograph Network (Data set), International Federation of Digital Seismograph Networks, doi:10.7914/SN/CR.

Yuhi, M., S. Umeda, M. Arita, J. Ninomiya et al. (2024). Dataset of post-event survey of the 2024 Noto peninsula earthquake tsunami in Japan, Sci. data, 11, 1, 786, doi:10.1080/21664250.2024.2368955.

ZAMG – Zentralanstalt für Meterologie und Geodynamik (1987). Austrian Seismic Network (Data set), International Federation of Digital Seismograph Networks, doi:10.7914/SN/OE.

***CORRESPONDING AUTHOR: Johannes STAMPA**,
Kiel University, Institute of Geosciences, Kiel, Germany
e-mail: johannes.stampa@ifg.uni-kiel.de